JOURNAL OF GEOPHYSICAL RESEARCH, VOL. 105, NO. D17, PAGES 22,427–22,436, SEPTEMBER 16, 2000

Use of Doppler radar to assess ice cloud particle fall velocity–size relations for remote sensing and climate studies

Sergey Y. Matrosov

Cooperative Institute for Research in Environmental Sciences, University of Colorado, Boulder
NOAA Environmental Technology Laboratory, Boulder, Colorado

Andrew J. Heymsfield

National Center for Atmospheric Research, Boulder, Colorado

Abstract. Knowledge of ice crystal terminal velocities, both for individual crystals and for size distributions, is important for an adequate representation of ice particle sedimentation in climate models. While the terminal velocities (v_t) of individual crystals of simple shapes have been measured, theoretical relations of the form $v_t = AD^B$ (where D is the maximum particle dimension), obtained using expressions for the aerodynamic drag force, are often more useful because they can be applied to a wide range of particle sizes and heights and temperatures in the atmosphere. For high tropospheric ice clouds the coefficient A has been found to vary over 1 order of magnitude; the exponent B is generally within the range 0.7–1.4. Aerodynamic drag force calculations show that A and B are related. A and B can also be used to characterize terminal-velocity–particle characteristic size relations for size distributions. In this study we use collocated, vertically pointing measurements of ice cloud radar reflectivity, Doppler velocity, and IR brightness temperatures to estimate the vertical profiles of cloud particle characteristic size, cloud ice water content, and vertically averaged value of the coefficient A, emphasizing cirrus clouds. We analyze variations in terminal-velocity–size relations for individual particles and corresponding variations for ensembles of particles: for example, in relations between the reflectivity-weighted terminal velocity and the median volume size and between the mass-weighted terminal velocity and the median volume size. The retrievals indicate that A ranges from ~250 to almost 4000 (cgs units), similar to the range found from the theoretical calculations. The coefficient A tends to decrease as a characteristic particle size (e.g., median size) increases. As a simplification for climate modeling efforts, we present an empirical relation between median size and A, although there is a fair amount of variability about this relation. Using the Doppler measurements and retrieval data, we also derive relations between the mass-weighted terminal velocity and cloud ice water content. Such relations are useful for representing fallout of ice particles in climate and cloud-resolving models.

1. Introduction

Unlike water drops, ice particles of a given size falling at a particular height can have very different terminal velocities, depending on their shape (habit), bulk density, and fall attitude. For the common types and sizes of particles found in high-altitude ice clouds such as cirrus, terminal velocities of individual particles can vary from few centimeters per second to about 1 m s^{-1}. These velocities have been measured (mostly for large ice particles such as snowflakes) or derived theoretically using expressions for the aerodynamic drag force and empirical relations between particle mass and size and particle projected area and size. The results of both calculations and experimental studies are usually expressed in a power-law form. A list of relevant theoretical studies is given by *Mitchell* [1996].

Knowledge of the terminal velocities of individual ice crystals, or of mean values that represent size distributions, are both important for cloud and climate modeling [e.g., *Starr and Cox*, 1985]. Ice clouds, especially cirrus, have been recognized for their relevance to the radiative balance of the Earth's atmosphere. The radiative impact of cirrus clouds is determined, in part, by the significant temporal persistence and spatial extent of this cloud type. The crystal fall velocities are a key element which determines the lifetime and spatial extent of these clouds. Vertical air motions modulate the fall velocities, but over the course of a cloud's lifetime, the net particle velocities are positive downward. Cirrus clouds also affect the climate system indirectly through the vertical redistribution of atmospheric water vapor [*Petch et al*., 1997].

The use of millimeter wavelength Doppler radar provides a powerful tool for measuring cloud properties. These radars, by themselves and especially in combination with other instruments, can be used effectively for remote sensing of microphysical parameters in ice and liquid water clouds [e.g., *Kropfli et al*., 1995]. In a vertically pointing mode and with proper time averaging (of the order of several hours), to remove small-scale air vertical motions, the measured Doppler velocity can be used to estimate the reflectivity-weighted cloud particle termi-

Copyright 2000 by the American Geophysical Union.

Paper number 2000JD900353.
0148-0227/00/2000JD900353$09.00

nal velocity. Very often, this velocity exhibits a good correlation with reflectivity and cloud temperature, and a relation between these parameters can be obtained for a particular period of study [*Orr and Kropfli*, 1999]. Such a relation derived for a particular cloud allows estimation of quasi-instantaneous vertical profiles of reflectivity-weighted particle terminal velocities.

Measurements taken with a vertically pointed Doppler radar and coincident estimates of cloud optical thickness from IR brightness temperature can be used to retrieve vertical profiles of microphysical parameters such as particle characteristic size and cloud ice water content [e.g., *Matrosov*, 1997]. These microphysical parameters can then be related to concurrent estimates of reflectivity-weighted terminal velocity. Such an approach provides a new way of obtaining observational terminal velocity–characteristic size and terminal velocity–cloud ice content relations for clouds with the variety of crystal habits that often coexist. The observational relations from remote sensing measurements can then be compared with those available from model calculations for idealized crystal shapes. The variability in parameters of these relations can be assessed, and recommendations can be made for the use of such relations in cloud and climate modeling.

In this study we apply the remote sensing approach to upper troposphere ice cloud measurements from a suite of remote sensing instruments from the National Oceanic and Atmospheric Administration (NOAA) Environmental Technology Laboratory (ETL). These data were obtained during several field campaigns, including the First International Satellite Cloud Climatology Project (ISCCP) Regional Experiment (FIRE II) [*Stephens*, 1995], the Atlantic Stratocumulus Transition Experiment (ASTEX) [*Randall*, 1995], the 1995 Arizona Program [*Klimovski et al*., 1998], and the Atmospheric Radiation Measurement (ARM) Program [*Stokes and Schwartz*, 1994] intensive operation periods (IOPs).

2. Variability of Theoretical Terminal Velocity–Size Relations

For an individual ice particle with size D (usually given as the maximum particle dimension), a parameterized expression for terminal velocity v_t can be given as [*Mitchell*, 1996]

$$v_t = a\,\nu(2\alpha g/\rho_a \nu^2 \gamma)^b D^{b(\beta+2-\sigma)-1}, \tag{1}$$

where g, ν, and ρ_a are the gravitational acceleration, the kinematic viscosity, and the air density, respectively. Note that the kinematic viscosity is proportional to the reciprocal of the air density: $\nu = \eta/\rho_a$, and the dynamic viscosity η depends only on temperature. In (1), a, b, α, β, γ, and σ are the coefficients and exponents in empirical mass (m) and projected to the flow area (P)-dimensional, and Reynolds (Re) − Best(X) number power-law expressions:

$$Re = aX^b, \tag{2}$$

$$m = \alpha D^\beta, \tag{3}$$

$$P = \gamma D^\sigma. \tag{4}$$

The Best number has no dependence on the drag coefficient and terminal velocity:

$$X = (2g/\rho_a \nu^2)\, D^2 (m/P), \tag{5}$$

unlike the Reynolds number, which depends on terminal velocity:

$$Re = (v_t D)/\nu. \tag{6}$$

The a, b, α, β, γ, and σ depend on particle habits, aspect ratios, and density; also, within the same habit, they might be different for different intervals of D. However, as shown by *Mitchell* [1996], a and b in (2) can be considered to be approximately constant in four different intervals of the Best number X. The dependence of these parameters on particle habits within each interval can be neglected. For the fall regime with $10 < X \leq 585$, which is valid for most cirrus cloud particles, $a = 0.06049$ and $b = 0.831$.

Equation (1) can also be rewritten as a simple power-law function of D:

$$v_t = AD^B. \tag{7}$$

Mitchell [1996] summarized the power-law coefficients and exponents a, b, α, β, γ, and σ for various cloud particle habits in different size intervals and different fall regimes. According to (1), each set of these coefficients determines an individual terminal velocity–size relationship. We used Mitchells' data to calculate values of A and B in (7), where the particle major dimension is oriented perpendicular to its fall direction. The calculations were performed for a common altitude of high-altitude ice clouds at 8 km ($P = 350$ hPa), assuming $\rho_a = 0.00052$ g cm^{-3}, and $\eta = 0.000152$ g cm^{-1} s^{-1} (at −40°C). The results of these calculations are presented in Table 1 for particle habits found in high-altitude ice clouds.

Since the Best number X depends on particle mass and projected cross-sectional area, the interval $10 < X \leq 585$ (for which data in Table 1 are shown) corresponds to slightly different particle size intervals ($D_{\min}$, $D_{\max}$) for different particle habits. $D_{\min}$, corresponding to $X = 10$, ranges from about 60 to 90 μm for the habits shown in Table 1. The values of $D_{\max}$ (for $X = 585$) usually vary from about 350 to about 550 μm. Particle size ranges in Table 1 correspond to the validity of the original mass-dimensional and projected area-dimensional relations from [*Mitchell*, 1996]. Note that for small hexagonal columns, $D_{\min} \approx 85$ μm, so the large value of A for small particles with this habit ($A \approx 12393$) is probably not very representative.

Table 1. Parameters in Terminal Velocity–Size Power Laws (Equation (7)) for Various Particle Types

Particle Type	A	B
Hexagonal plates (15 μm $< D \leq$ 100 μm)	2210	1.16
Hexagonal plates (100 μm $< D \leq$ 3 mm)	965	1.04
Hexagonal columns (30 μm $< D \leq$ 100 μm)	12393	1.42
Hexagonal columns (100 μm $< D \leq$ 300 μm)	1787	1.00
Hexagonal columns ($D >$ 300 μm)	348	0.48
Rimed long columns (200 μm $\leq D \leq$ 2.4 mm)	2055	0.98
Crystals with sector branches (Plb) (40 μm $\leq D \leq$ 2 mm)	281	0.70
Broad-branched crystals (P1c) (100 μm $\leq D \leq$ 1 mm)	271	0.71
Side planes (S1) (300 μm $\leq D \leq$ 2.5 mm)	1432	1.01
Bullet rosettes (5 branches) (200 μm $\leq D \leq$ 1 mm)	2476	1.23
Assemblages of planar polycrystals (20 μm $\leq D \leq$ 450 μm)	2296	1.13

Calculations made using data from [*Mitchell*, 1996]. Units are cgs.

Table 2. Parameters in Terminal Velocity–Size Power Laws (7) for Various Particle Types. Calculations made using data from *Heymsfield and Iaquinta* [2000]

Particle Type	A	B
Columns ($D \leq 350$ μm)	4124	1.31
Columns ($D > 350$ μm)	667	0.77
Bullets ($D \leq 540$ μm)	2282	1.19
Bullets ($D > 540$ μm)	574	0.72
Bullet rosettes ($D \leq 470$ μm)	1166	1.06
Bullet rosettes ($D > 470$ μm)	716	0.90

Units are cgs.

It can be seen from the data presented in Table 1 that particles found in ice clouds can exhibit a wide range of terminal velocity–size relations. The coefficient A can vary by more than 1 order of magnitude, though the exponent B shows variability centering around 1 and ranging from about 0.7–1.23 (excluding large hexagonal columns).

According to *Mitchell* [1996], different sets of coefficients a and b in (2) and (1) should be used for calculating terminal velocities for particles smaller than $D_{\min}$ or greater than $D_{\max}$. For the small-particle fall regime with $0.01 < X \leq 10$, $a = 0.04394$ and $b = 0.97$. The large-particle regime with $585 < X \leq 156{,}000$ corresponds to $a = 0.2072$ and $b = 0.638$. These two regimes correspond to size intervals from a few microns to $D_{\min}$ (i.e., $X = 10$) and from $D_{\max}$ (i.e., $X = 585$) to a few millimeters, respectively. Note that though there are typically many small particles present in cirrus, particles in the main fall regime ($10 < X \leq 585$) usually contribute most to the cloud radar measurables (i.e., reflectivity and Doppler velocity) and cloud ice water content.

The transition from the main particle fall regime ($10 < X \leq 585$) to the smaller particle fall regime ($0.01 < X \leq 10$) results in an increase of both the coefficient A and the exponent B in (7). The opposite is true for the transition from the main regime to the large-particle fall regime ($585 < X \leq 156{,}000$). This can be illustrated by an example of hexagonal plates. For plates in the small-particle fall regime, calculations yield $A \approx 4000$ and $B \approx 1.35$, and in the larger particle regime, plates are characterized by $A \approx 210$ and $B \approx 0.6$ (as opposed to $A \approx 965$ and $B \approx 1.04$ for the main regime).

The general tendency for the exponent B and coefficient A in the terminal-velocity–size relation (7) to diminish when particle size increases is valid for all particle habits. Furthermore, the relative increase of particle terminal velocity with size becomes smaller for larger particles, in part, because the bulk density decreases with particle size. These results are in agreement with recent findings by *Heymsfield and Iaquinta* [2000] who suggested the terminal velocity–size relations listed in Table 2.

The data from Tables 1 and 2 are shown in Figure 1 as a scatterplot. It can be seen from this figure that there is a good correlation between A and B. The best fit analysis yields: $B \approx 0.17\ A^{0.24}$ with a correlation coefficient of 0.9. Though the data in Figure 1 are for the main fall regime, the corresponding values for other regimes (e.g., $A \approx 4000$ and $B \approx 1.35$, and $A \approx 210$ and $B \approx 0.6$ for large and small hexagonal plates) are also well approximated by the best power law fit.

For a long time, theoretical calculations resulting in terminal velocity–size relations such as those discussed above were the main source for terminal velocity data in cloud models. Now these data can be supplemented by information about such relations obtained from Doppler radar measurements. Since single polarization radar measurements do not readily contain information on particle shape, it is convenient for the purpose of analyzing radar data to express particle sizes in terms of equivalent spherical diameters. The majority of common cirrus crystals contributing most to ice content and radar reflectivity have irregular quasi-spherical shapes in the sense that their dimensions along different directions are close to each other (e.g., polycrystals, bullet rosettes), and those dimensions D are close to the diameter of the circumscribed sphere. This notation for particle sizes will be used in this paper hereinafter.

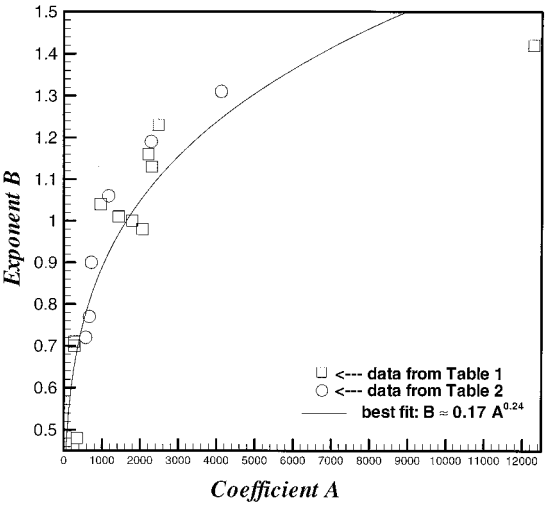

Figure 1. Relation between theoretical predictions of the coefficient A and the exponent B in equation (7). Units are cgs.

Since the radar wavelength is usually much larger than typical cloud particle sizes, it does not resolve the fine structure of these particles. Complex particles are seen by the radar as homogeneous scatterers with diminished bulk density rather than separate entities of solid ice and air pockets. Particle bulk density here is the ratio of the particle mass to the volume of that sphere.

3. Variability of Terminal Velocity–Size Relations From Remote Measurements

3.1. Reflectivity-Weighted Terminal Velocities for an Ensemble of Particles

The Doppler velocity (V_D) measured by a radar pointed vertically is the sum of the vertical air motion (V_a) and the reflectivity-weighted particle terminal fall velocities (V_Z): $V_D = V_a + V_Z$. *Orr and Kropfli* [1999] suggested an approach to estimate V_Z by assuming that the V_a cancels out (or at least it is small compared to V_Z) if measurements of V_D are averaged over a sufficiently long time interval (about several hours). Averaging is performed for small cloud height and cloud reflectivity bins, and regressions between the averaged V_D (which is an approximation for V_Z, in this case) and reflectivity (Z_e) measurements are obtained through the cloud depth. These case-dependent regressions can then be used to estimate the instantaneous vertical profiles of reflectivity-weighted particle terminal velocity from each profile of measured Z_e. It has been shown that this approach usually pro-

vides reasonable estimates of V_Z for clouds with no strong updrafts/downdrafts (less than about 1 m s^{-1}).

A general expression for V_Z can be given as

$$V_Z = \frac{\int_0^\infty v_t S_Z(v_t)\, dv_t}{\int_0^\infty S_Z(v_t)\, dv_t}, \tag{8}$$

where S_Z is the Doppler spectrum in the velocity domain. In the Rayleigh-scattering regime, which is approximately valid for particles smaller than about 1 mm at K_a-band radar frequencies ($\lambda \sim 8$ mm), (8) can be rewritten in the size domain

$$V_Z = \frac{\int_0^\infty K(\rho)Q(r)AD^B N(D)D^6\, dD}{\int_0^\infty K(\rho)Q(r)N(D)D^6\, dD}, \tag{9}$$

where $N(D)$ is the particle size distribution (PSD), and K and Q describe reflectivity corrections due to changing particle bulk density ρ and shape, respectively. Since ice cloud particles are usually much smaller than the radar wavelength, the shape dependence of measured radar parameters for a given particle class (either prolate or oblate) can be approximately described as a function of only one parameter, i.e., the particle aspect ratio (r in (9)). Note that polycrystal and bullet-rosette particles with $r \approx 1$ constitute a substantial, even predominant, component of the crystal population in many cirrus clouds.

The parameter K accounts for changes in the complex reflective index of ice, m_i, relative to that of water, m_w:

$$K = \frac{|(m_i^2 - 1)(m_i^2 + 2)^{-1}|^2}{|(m_w^2 - 1)(m_w^2 + 2)^{-1}|^2}. \tag{10}$$

It can be shown [e.g., *Atlas et al*., 1995] that

$$K \approx 0.23\rho^2. \tag{11}$$

The denominator of (9) represents the radar reflectivity Z_e. If one assumes that particle bulk density, shape, and coefficients A and B do not change with size and that the PSD can be satisfactorily described by the gamma function distribution $[N(D) = N_0 D^n \exp(-(3.67 + n)/D_0]$, (9) can be reduced to

$$V_Z = A[\Gamma(n + 7 + B)/\Gamma(n + 7)]D_0^B(3.67 + n)^{-B}, \tag{12}$$

where Γ is the gamma function, n is the order of this distribution, and D_0 is the median volume diameter, a parameter describing the whole PSD.

It can be seen from (12) that the transformation of the terminal velocity–size relationship for an individual particle (7) to one for the ensemble of particles (in terms of the reflectivity-weighted fall velocity and median size) effectively results in the change of the coefficient by a factor a_1:

$$V_Z = Aa_1(B)D_0^B. \tag{13}$$

Figure 2 shows a_1 as a function of the exponent B for the approximate range of B predicted by theoretical calculations (see Tables 1 and 2). The data in this figure are presented for 3 orders of the gamma function PSD ($n = 0, 1, 2$). These 3 orders were shown to satisfactorily describe experimental PSD in ice clouds [*Kosarev and Mazin*, 1991]. It can be seen that a_1 increases with the exponent B by 40–50% over the range of typical changes in B (0.7–1.3). Variability of a_1 due to the PSD shape also increases with B. Using the relation between A and B (i.e., $B \approx 0.17\, A^{0.24}$), corresponding values of A are also shown along the abscissa in Figure 2.

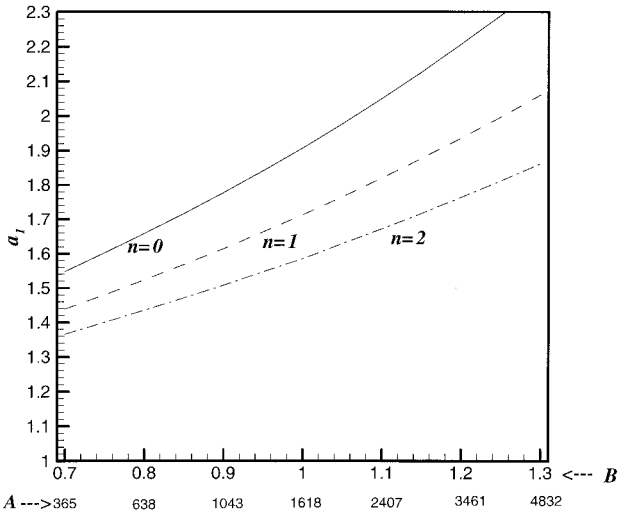

Figure 2. Coefficient a_1 as a function of the exponent B for different orders of n of the gamma function size distribution assuming constant bulk density of cloud particles. Values of the coefficient A are also shown (from $B = 0.17\, A^{0.24}$).

Although, as mentioned before, the majority of cirrus particles are characterized by $r \approx 1$, for the sake of generality, we analyze here the nonsphericity parameter $Q(r)$. This parameter $Q(r)$ in the general expression (9) accounts for the fact that nonspherical particles usually scatter radiation stronger than equal-volume spheres. This fact was mentioned first by *Atlas et al*. [1953]. For the density of solid ice, these authors compared the radar reflectivity of randomly oriented oblate and prolate particles with that of spheres. Since larger particles (greater than about 100 μm [e.g., *Mitchell*, 1996]) which contribute most in the radar parameters tend to be oriented with their major dimensions in the horizontal plane, we performed such estimations for different bulk densities and particles randomly oriented horizontally.

Figure 3 shows the shape parameter Q in (9) calculated here using the Rayleigh-scattering theory for spheroids [e.g., *Bohren and Huffman*, 1983] as a function of aspect ratio r for prolate (e.g., bullets, columns, needles) and oblate (e.g., plates, dendrites) types of ice particles. It can be seen from this figure that the nonsphericity effects are stronger for oblates than for prolates. These effects diminish very rapidly as the particle bulk density decreases. The results of Figure 3 can be approximated for $r \geq 0.1$ by a power-law function as

$$Q = r^{-0.41\rho} \quad \text{(oblates)}, \tag{14}$$

$$Q = r^{-(0.26\rho - 0.03)} \quad \text{(prolates)} \qquad (\rho \text{ in g cm}^{-3}). \tag{15}$$

It is more realistic to assume that the bulk density ρ decreases with particle size. With this assumption a size dependence of the parameters K and Q in (9) is introduced (through the size dependence of bulk density). The bulk density of smaller particles (less than $\sim$100 μm) is close to that of solid

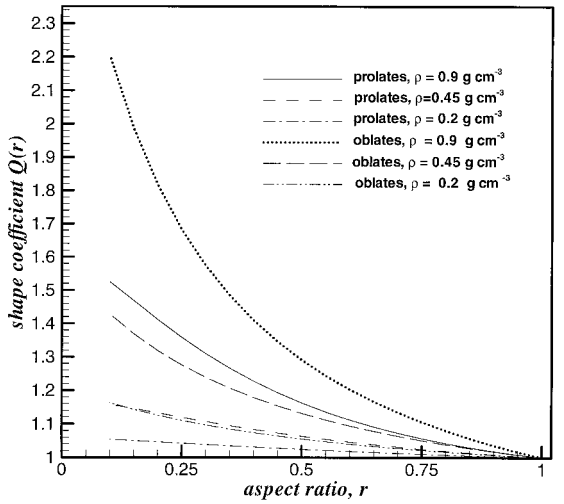

Figure 3. Nonsphericity correction for radar reflectivity (Q) as a function of particle aspect ratio for different particle bulk densities.

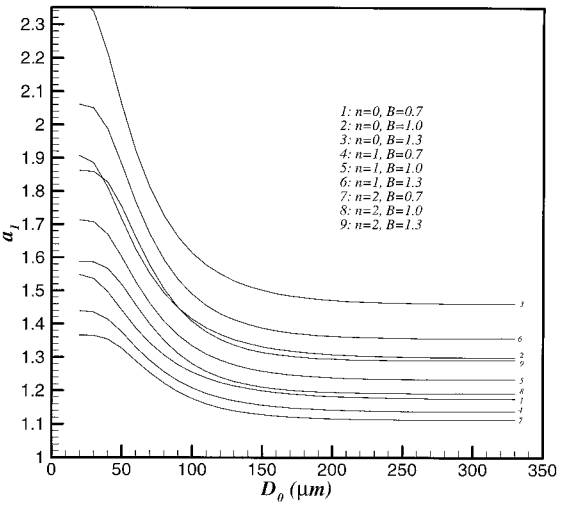

Figure 5. Coefficient a_1 as a function of particle median volume size for different orders of the gamma function size distribution (n) and exponents B.

ice [*Heymsfield*, 1972]. For larger particles the effective bulk density is proportional approximately to the reciprocal of the (3-β)-th power of particle size: $\rho \sim 1/D^{3-\beta}$, and β is about 2 for different particle habits [*Mitchell*, 1996; *Brown and Francis*, 1995; *Heymsfield and Iaquinta*, 2000]. The assumption of a density decrease with size results in a decrease of a_1 compared to the case ρ = const shown in Figure 2.

This is illustrated in Figure 4 which, like Figure 2, depicts a_1 as a function of B but for the case of the bulk density which decreases with particle size. A value of $\beta = 1.9$ was assumed for the mass-size relation (3) as suggested by *Brown and Francis* [1995]. The data are presented for oblate and prolate particles with aspect ratio $r = 0.5$. It can be seen that the shape factor does not affect the results significantly since the effects of K on V_Z are more pronounced than those of Q in (9).

For ρ = const, a_1 does not depend on the particle median size D_0. When the density changes with particle size, however, there is such a dependence. The results in Figure 4 were obtained for $D_0 = 100$ μm. To assess the effect of a decrease of a_1 with an increase of D_0, calculations of a_1 as a function of D_0 were performed for various values of B and n. The results of these calculations are shown in Figure 5.

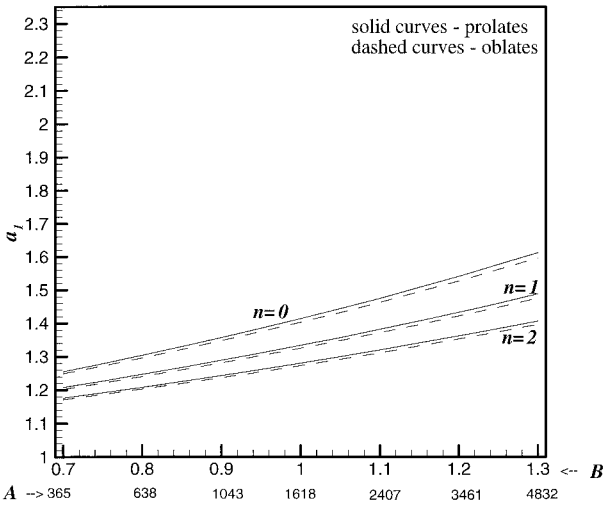

Figure 4. Same is in Figure 2 but for the bulk density changing with particle size and nonspherical particles with aspect ratio of 0.5 ($D_0 = 100$ μm).

At the lower end of D_0 in Figure 5, values of a_1 approach those shown in Figure 2. This is explained by the fact that for $D_0 < 30$ μm, the particle bulk densities are almost equal to that of solid ice, since at these values of median volume size, few of the individual particles in the distribution exceed 100 μm in size. As the median size of the particle ensemble increases, a_1 reaches asymptotic values that depend on B and n.

Combined analyses of data in Figures 2–5 show that the transition from the terminal velocity–size relation for an individual particle ($v_t = AD^B$) to such a relation for an ensemble of particles in terms of reflectivity-weighted particle terminal velocity V_Z and median particle size D_0 results in an increase of the coefficient A by factor (a_1), which can change from about 1.1 to about 2.3. Larger increases are for smaller particles because they have larger bulk densities and larger values of the exponent B. These relative changes (1.1 to 2.3) are still much smaller than the natural variability of the coefficient A due to changes in particle habits (see Tables 1 and 2).

3.2. Radar-Radiometer Method

The radar-radiometer method for remote sensing of ice clouds uses collocated measurements taken by a vertically pointed radar (typically K_a-band radar) and a narrowband ($\lambda \sim 10$–11.4 μm) IR radiometer. This method uses vertical profiles of radar reflectivity Z_e and reflectivity-weighted particle terminal velocities V_Z (using the approach from *Orr and Kropfli* [1999]) in combination with estimates of cloud IR optical thickness from radiometer measurements for retrieving vertical profiles of ice cloud microphysical parameters through an iterative process [*Matrosov*, 1997].

For an assumed type of PSD (e.g., the first-order gamma function) the retrieved microphysical properties include vertical profiles of cloud ice water content (IWC) and particle median size (in terms of either median volume size D_0 or median mass size D_m). In the first iteration a vertical profile of particle median sizes is obtained from V_Z for an assumed value

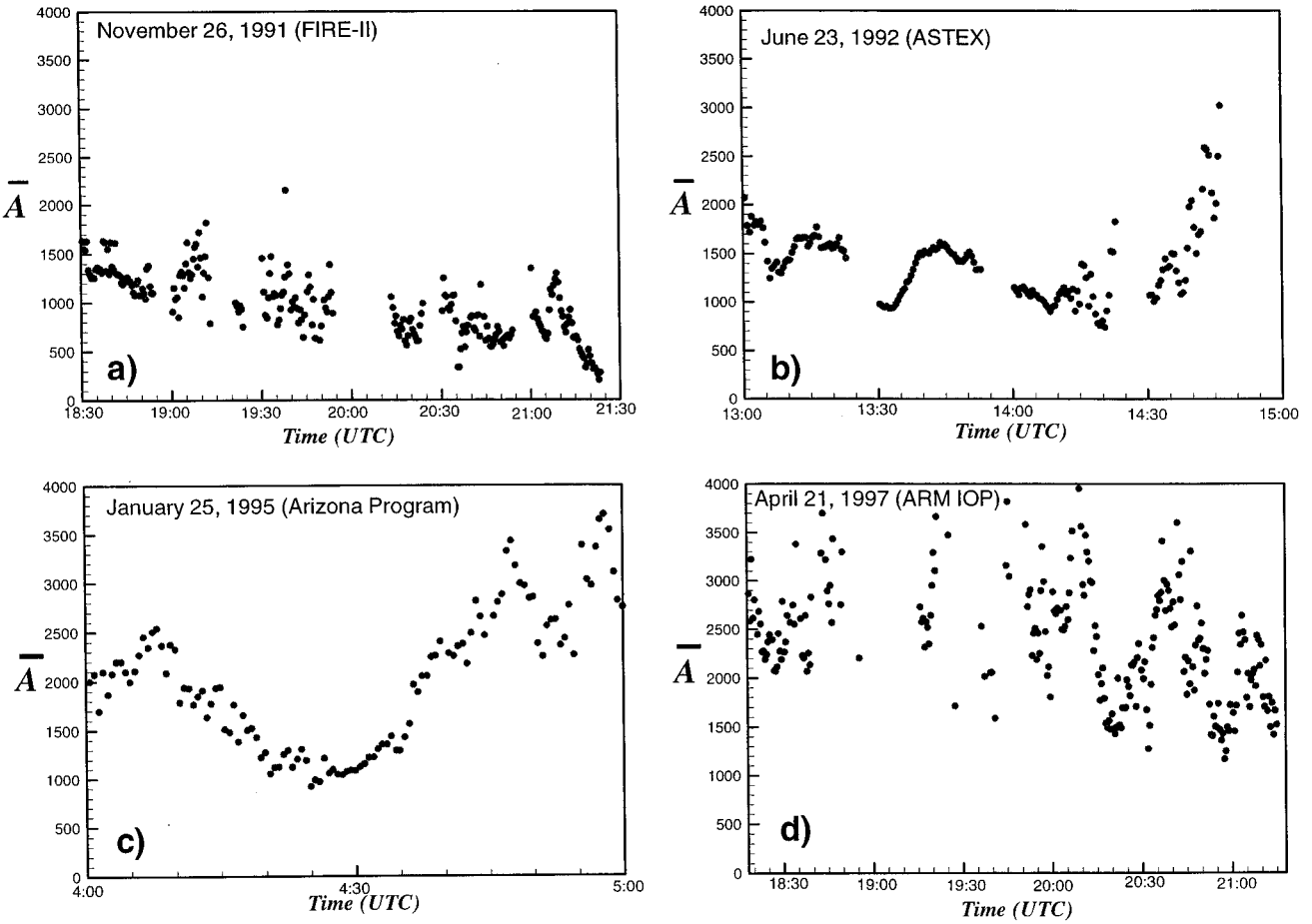

Figure 6. Time series of mean retrieved values of the coefficient A ($\bar{A}$) in particle terminal velocity–size relations for different observations of ice clouds.

of A (and B through $B \approx 0.17\,A^{0.24}$) in the terminal velocity–size relation, and a profile of IWC is then calculated from reflectivity measurements using the equation *Atlas et al.* [1995]:

$$Z_e = G\ \mathrm{IWC}\ D_0^3, \tag{16}$$

where G depends on the shape of PSD (i.e., n) and on the assumption of particle bulk density as a function of size. The detailed analysis of the parameter G is given by *Matrosov* [1999].

For the retrieved profiles of D_0 and IWC a profile of the cloud absorption coefficient is then calculated, and its vertical integral (i.e., absorption optical thickness) is compared with the radiometric estimate of cloud optical thickness. The calculated and measured optical thicknesses are forced to agree by changing the value of A (and hence B) for the next iteration. The iterations are stopped when the calculated and measured optical thicknesses are within 5%, which is of the order of the uncertainty of the measured optical thickness. At all iteration steps the exponent B is assumed to be related to A as shown by the best fit in Figure 1. $A = 1500$ (cgs units) is usually used for the initial guess and it generally takes about 3–4 iterations for the convergence of the iteration process.

The microphysical retrieval results of IWC and median size for high-altitude ice clouds using the radar-radiometer method were compared to aircraft-based in situ measurements of these cloud parameters [*Matrosov et al.*, 1995, 1998]. These comparisons showed good agreement, and deviations between direct and remote measurements were generally within the uncertainties of both types of measurements. More details of the radar-radiometer method for retrieving vertical profiles of median size and IWC and a value of A in high-altitude ice clouds are given by *Matrosov* [1997].

3.3. Results of Retrievals of the Coefficient A Using the Radar-Radiometer Method

Particle habits in ice clouds can change with altitude and can vary within a single radar resolution volume. Unlike for IWC and particle median size, the radar-radiometer method does not facilitate vertically resolved retrievals of the coefficient A, and the retrieval results represent just one vertically averaged value $\bar{A}$ for each vertical profile of radar measurements.

Figure 6 shows the results of the retrievals of coefficient $\bar{A}$ for four representative cases of ice cloud observations from the ETL field experiments mentioned in section 1. In the cases shown, collocated microwave radiometer measurements indicated no presence of the liquid phase during the observations. The time resolution of each estimate of $\bar{A}$ is 30 s. The times of missing data (e.g., around 2000 UTC during the November 26, 1991, case) correspond to intervals when the ice clouds were blocked from the IR radiometer view by patches of low-level liquid water clouds. During the retrievals it was assumed that the shape of the PSD is described by the first-order gamma

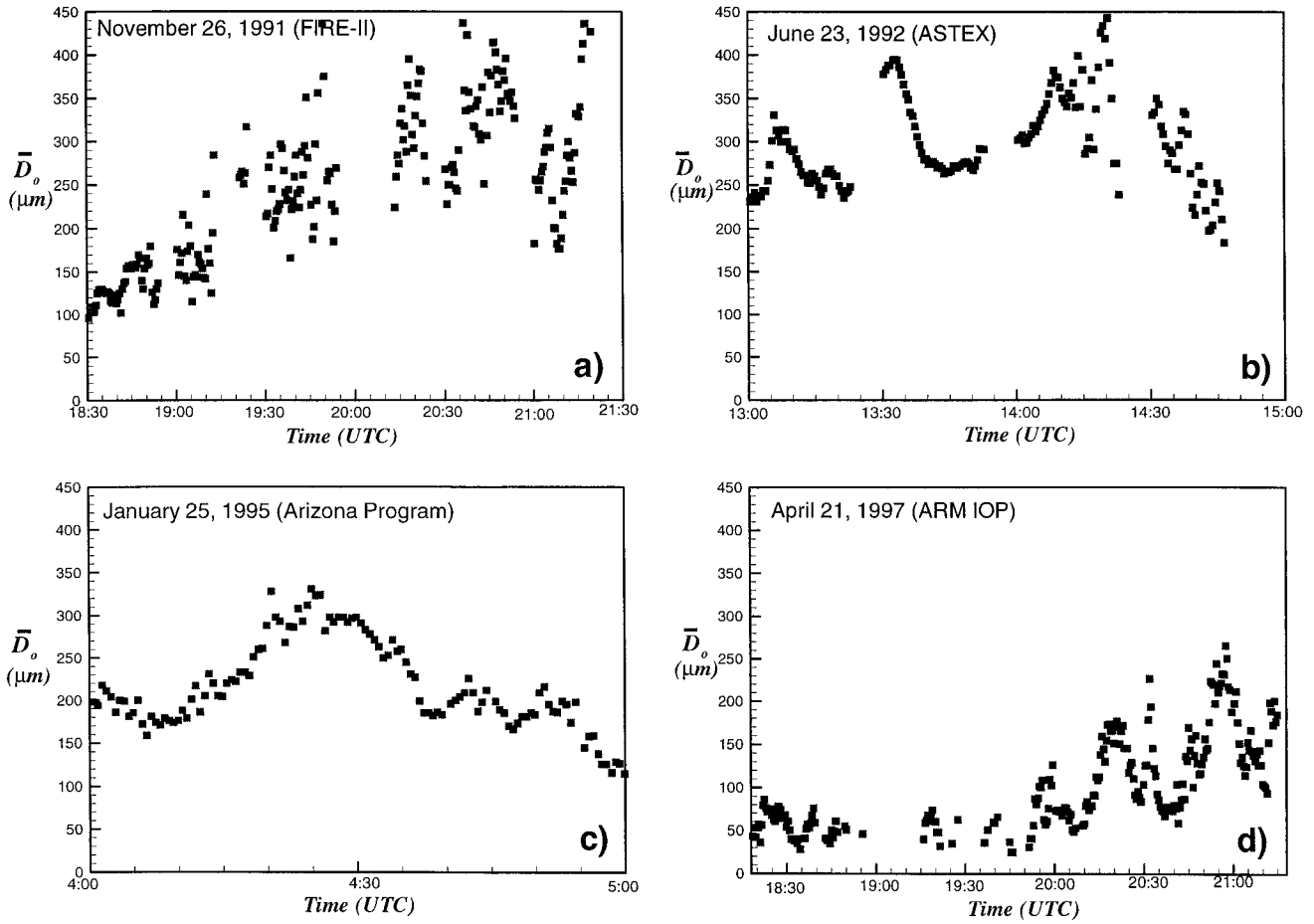

Figure 7. Same as in Figure 6 but for vertically averaged median size of cloud particles.

function, and the particle bulk density diminishes as -1.1 power for larger particles ($D > 100$ μm) as in the work of *Brown and Francis* [1995].

The retrieval results were normalized, as were the data in Tables 1 and 2, to an altitude of 8 km. The height dependence of $\bar{A}$ due to air density and viscosity changes (not due to particle habit changes) was accounted for by the expression [*Pruppacher and Klett*, 1978]:

$$\bar{A} = \bar{A}_0(\rho_a/\rho_{a0})^{\varepsilon-1}/(\eta/\eta_0)^{1-2\varepsilon}, \quad (17)$$

where the subscript "0" refers to the reference altitude values. Coefficient ε is fairly independent of particle habit and is about 0.9 for smaller particles ($0.1 < Re < 4$), decreasing to 0.75 for larger particles ($4 < Re < 20$).

The observational cases presented in Figure 6 comprise a variety of microphysical conditions. The clouds during these cases were rather thick and were located between about 5 and 10 km above ground level (agl). The retrieved values of IWC for these ice clouds varied mostly between 0.001 and 0.1 g m^{-3}. The vertical distributions of retrieved IWC in the ASTEX, FIRE-II, and Arizona program cases are presented in Figure 3 by *Matrosov* [1997].

It can be seen from Figure 6 of this paper that in the ASTEX and Arizona program cases, $\bar{A}$ changes quite gradually, while in the other two cases (especially in the ARM IOP case), more rapid changes in $\bar{A}$ are evident. This shows a higher relative variability of the cloud properties. The November 26, 1991, FIRE-II case exhibits a gradual decline of $\bar{A}$. This case was characterized initially by high cirrus clouds. As a cold front moved in, cloud bases became lower, reaching about 5 km agl at around 2130 UTC.

According to the presented data, the dynamic range of variability in $\bar{A}$ is mostly between 250 and 4000 (cgs units), with the majority of data from 1000 and 2000. Such variability range is in good general agreement with theoretical calculations shown in Tables 1 and 2 for particle habits found most frequently in high-altitude ice clouds.

The smallest retrieved values of $\bar{A}$ are about 250, which agrees with the smallest theoretical values given in Table 1. Note, however, that such small observational values of $\bar{A}$ are associated with large particles, and $\bar{A}$ usually decreases as particle characteristic size increases. The largest experimental values of $\bar{A}$ were observed during the ARM IOP case (see Figure 6d) where the particles were generally smaller, as discussed later. The observed values of $\bar{A}$ for this case sometimes exceed theoretical predictions for the main cloud particle fall regime ($10 < X \leq 585$) but are well within predictions for the small-particle fall regime ($0.01 < X \leq 10$).

It is instructive to compare variations of $\bar{A}$ with changes in the characteristic particle size. Since $\bar{A}$ represents a vertically averaged value, it is logical to compare it with vertically averaged values of cloud particle characteristic size. Figure 7 shows the time series of the vertically averaged, IWC-weighted, particle median sizes $\bar{D}_0$ retrieved using the radar-radiometer

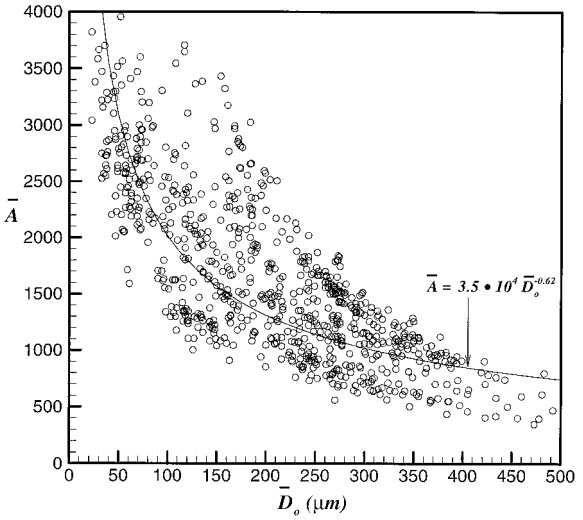

Figure 8. Scatterplot of vertically averaged values of $\bar{A}$ (cgs units) and median volume size of cloud particles $\bar{D}_0$, as determined by the radar-radiometer remote sensing method.

method for the same ice cloud events as in Figure 6. Values of $\bar{D}_0$ were obtained by averaging vertical profiles of retrieved median sizes (D_0) and represent a cloud particle characteristic size for the entire vertical profile.

Comparisons of Figures 6 and 7 reveal a noticeable anticorrelation between the coefficient $\bar{A}$ and the particle characteristic size $\bar{D}_0$. This fact is in accord with theoretical data presented in Table 2 for different size intervals of particles with the same habit. In spite of this anticorrelation, however, the median size does not determine the value of the coefficient $\bar{A}$ in a one-to-one manner. This can be seen by comparing data for the beginning of the Arizona Program and the ARM IOP cases, when similar values of $\bar{A}$ (about 2000) resulted from much different particle median sizes D_0. The later were smaller for the ARM IOP case by a factor of 2 to 3. The relatively large variability of $\bar{A}$ revealed by the experimental data indicates that there is no unique terminal-velocity–size relation that can suit all modeling needs. However, accounting for particle characteristic size can reduce, though not completely eliminate, the natural uncertainty of these relations.

Figure 8 presents the scatterplot of simultaneous estimates of $\bar{A}$ and $\bar{D}_0$ for the combined data set composed of the observational cases shown in Figures 6 and 7. The regression analysis of the data presented in Figure 8 yields the following best fit power-law relation between $\bar{A}$ and $\bar{D}_0$: $\bar{A} = 3.5 \times 10^4 \bar{D}_0^{-0.62}$ ($\bar{A}$ is in cgs units and $\bar{D}_0$ is in microns) with a correlation coefficient of about 0.7. It can be seen from Figure 8 that the data scatter in $\bar{A}$ are generally greater for smaller values of $\bar{D}_0$, which could be, in part, explained by higher relative errors in measurements of small Doppler velocities. The rate of fall velocity increase with particle size diminishes as particles grow larger and their bulk density decreases. This is reflected in anticorrelation between $\bar{D}_0$ and $\bar{A}$. As mentioned before, the dynamic range of remotely estimated values of $\bar{A}$ is in good agreement with the theoretical predictions summarized in Tables 1 and 2.

The retrievals of $\bar{A}$ and $\bar{D}_0$ shown above were performed assuming the first-order gamma function type of PSD ($n = 1$) and quasi-spherical particles ($r = 1$). Sensitivity tests indicate that changing these assumptions in the ranges $0 \le n \le 2$ and $0.3 \le r \le 1$ could result in about 20% changes in the retrieved values of $\bar{A}$ and $\bar{D}_0$. Retrieval uncertainties of such magnitude are still much smaller than the dynamic range in the natural variability of $\bar{A}$ and $\bar{D}_0$.

4. Terminal Velocity–Ice Mass Content Relations

Describing the rate of cloud particle fallout is important for climate model studies. Some cloud models handle this mechanism through relations between the mass-weighted particle terminal velocities and the cloud ice water content (IWC) or ice mass mixing ratio [e.g., *Starr and Cox*, 1985]. For simplicity the terminal velocities are often set to a constant positive value or zero. The model output depends significantly on the relations and/or constant values assumed for the mass-weighted terminal velocities [*Petch et al*., 1997]. Measurements of the particle terminal velocities using the Doppler radar, coupled with simultaneous estimates of cloud IWC from the radar-radiometer method, can be used to devise these relations.

4.1. Reflectivity-Weighted Versus Mass-Weighted Terminal Velocities

Analogous to (9), the mass-weighed particle terminal velocity can be given as

$$V_m = \frac{\int_0^\infty \rho A D^B N(D) D^3 \, dD}{\int_0^\infty \rho N(D) D^3 \, dD}. \tag{18}$$

Since V_m is of main interest, for cloud-modeling purposes, while radar provides the reflectivity-weighted terminal velocities V_Z, it is instructive to estimate the ratio of these velocities:

$$a_2 = V_Z / V_m. \tag{19}$$

The coefficient a_2 depends on the same parameters as the coefficient a_1. The variability of a_2 was analyzed analogously to that of a_1 as a function of particle median size D_0 (see Figure 5). The results of modeling for different assumed orders of the gamma function PSD and values of the exponent B are shown in Figure 9.

The reflectivity-weighted terminal velocities are greater than the mass-weighted velocities. The variability of a_2 is less than that for a_1. Values of a_2 are mostly between 1.2 and 2. As in the case with a_1, the coefficient a_2 approaches values for the constant particle bulk density as D_0 decreases to less than about 30 μm.

From (13) and (19), one can obtain

$$V_m = A(a_1/a_2) D_0^B. \tag{20}$$

It can be seen by comparing Figures 5 and 9 that the ratio (a_1/a_2) is close to 1 for smaller particles (50 μm $< D <$ 100 μm), so for this size range, the coefficients of terminal velocity–size relations for individual particles can be used with good accuracy to describe such relations in terms of the mass-weighted terminal velocities and particle median volume sizes if the particle habit is assumed to be constant. Since both a_1 and a_2 depend slightly on B, D_0, and n, model calculations of this ratio were performed (not shown here) for $0.7 \le B \le 1.3$, 20 μm $\le D_0 \le$ 500 μm, and $0 \le n \le 2$. These

calculations indicate that for larger-particle populations ($D_0 >$ 200 μm) the ratio (a_1/a_2) is about 0.8, so the mass-weighted fall velocities are about 80% of the fall velocity of an individual particle whose size is equal to the median volume size of the population D_0. Note that D_0 are substantially greater than the modal size D_{mod}, which is defined as the size where the size distribution function reaches its maximum value. For the first and second orders of the gamma-function size distributions $D_{\mathrm{mod}} \approx 0.21\ D_0(n = 1)$ and $D_{\mathrm{mod}} \approx 0.35\ D_0(n = 2)$, respectively.

4.2. V_m-IWC Relations

To illustrate possibilities of constructing V_m-IWC relations from data obtained using the remote sensing method, we present a scatterplot in Figure 10 for the ASTEX June 23, 1992, case where retrieved IWC values are plotted against corresponding values of V_m. Here again, vertical profiles of IWC and V_Z were obtained using the radar-radiometer method and the approach by *Orr and Kropfli* [1999], respectively. Values of V_m were calculated from estimates of V_Z using the coefficients a_1 and a_2 from Figures 5 and 9. As before, during the microphysical retrievals it was assumed that the shape of the PSD is that of the first-order gamma function ($n = 1$), and the exponent B is related to the coefficient A by means of the best power-law fit $B = 0.17\ A^{0.24}$. These assumptions determined values of the coefficient a_2 for conversions of vertical profiles of V_Z to vertical profiles of V_m. Note that for typical particle median sizes D_0 during this case (see Figure 7b) $V_m \approx 0.65\ V_Z$.

Each scatterplot dot in this figure represents IWC and V_m values estimated with the 30 s temporal and the 37.5 m spatial resolutions. IWC in high-altitude ice clouds can vary as much as 4 orders of magnitude [*Dowling and Radke*, 1990]. For the observations presented here, however, the majority of the retrieved IWC values were in the interval from about 0.002 to 0.2 g m^{-3}. The relative lack of data with very small values of IWC is explained by the current sensitivity of the radar used for these measurements (−30 dBZ at 10 km range) and hence its inability to observe very tenuous clouds with small ice contents.

An empirical best fit power-law approximation,

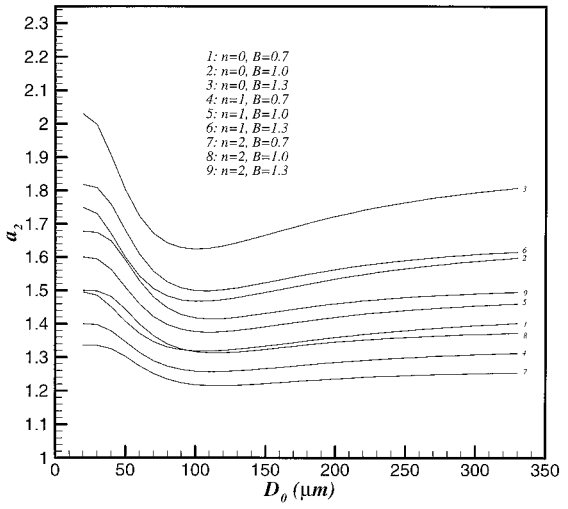

Figure 9. Ratio, a_2, between reflectivity-weighted and mass-weighted particle terminal velocities as a function of particle median volume size D_0.

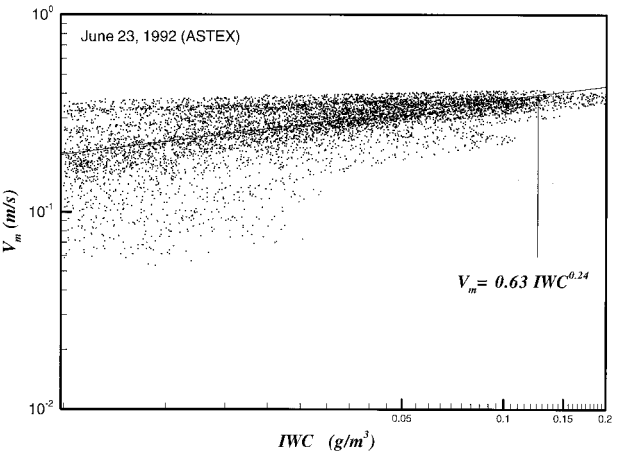

Figure 10. Scatterplot of mass-weighted particle terminal velocities V_m versus cloud IWC for an ice cloud observed on June 23, 1992, during ASTEX.

$$V_m = \xi \mathrm{IWC}^{\aleph}, \tag{21}$$

was derived for this observational case ($\xi \approx 0.63$ and $\aleph \approx 0.24$ if IWC is in g m^{-3} and V_m is in m s^{-1}). Mass-weighted terminal velocities increase with IWC since higher values of cloud mass are, on average, associated with larger particles which have greater terminal velocities. These larger particles also exhibit smaller variations in terminal velocities. This is one factor which results in a relative decrease of data scatter as IWC increases. The largest data scatter is seen for small cloud contents which, in part, can be attributed to larger relative uncertainties in measuring small amounts of IWC and small terminal velocities. Note that assumption of $n = 2$ or $n = 0$ rather than $n = 1$ will result in about 20% increase (for $n = 2$) or 20% decrease (for $n = 0$) of V_m values relative to those calculated from (21) using $\xi \approx 0.63$ and $\aleph \approx 0.24$.

A general increase of V_m with IWC is not very pronounced, however, which can be explained by the tendency for dV_t/dD to decrease with increasing particle size. The exponent $\aleph$ and the coefficient ξ in (21) exhibit a noticeable variability from case to case. For the observational case considered here ξ was changing form about 0.4 to about 0.65 and $\aleph$ was changing from about 0.17 to about 0.35. The variability of ξ and $\aleph$ due to the assumption of n ($0 \le n \le 2$) is less than the variability in these quantities on the case-to-case basis.

5. Conclusions

Theoretical calculations of ice particle terminal velocities as a function of size indicate large variability in the relations $v_t = AD^B$ for common ice cloud particle types. According to these calculations the variability of the coefficient A can exceed 1 order of magnitude (generally 270–4300 in cgs units) for the main fall regime with Best numbers X between 10 and 585. The coefficient A could reach even greater values for a small-particle fall regime ($0.01 < X \le 10$). The exponent B varies usually from about 0.7 to 1.4. There is a correlation between A and B, and both parameters have a tendency to decrease when particle size increases, so the rate of increase of v_t decreases with particle size.

It has been shown that the transition from the terminal velocity–size relation for an individual particle to that for an

ensemble of particles results in an effective increase of the coefficient A if the relation is considered in terms of reflectivity-weighted terminal velocities (V_Z) and median volume particle sizes D_0. The corresponding increase amounts to a factor of 1.1–2.3, depending on the details of the particle size distribution and density.

Measurements taken by vertically pointed Doppler radar in combination with collocated IR radiometer data from different field programs provided an opportunity to experimentally estimate the parameters of the terminal velocity–size relations. The Doppler radar data were used to estimate the reflectivity-weighted terminal velocities of cloud particles and the retrievals from the radar-radiometer method were used to estimate the particle median sizes and cloud IWC. On the basis of these data the vertically averaged values of the coefficient A (i.e., $\bar{A}$) in the terminal velocity–size relation were estimated for representative high-altitude (5.5–10.5 km) ice cloud cases. These experimentally estimated values of $\bar{A}$ exhibited variability in the approximate range from 250 to 4000 (cgs units), with the majority of estimates between 1000 and 2000. Such a variability is in good agreement with theoretical predictions, given uncertainties in the details of the particle size distributions and transitions between different fall regimes of cloud particles.

According to the retrieval results, a noticeable negative correlation was present between $\bar{A}$ and vertically averaged particle median size $\bar{D}_0$. This is a result of particle fall velocities growing with particle size at a slower rate as particles become larger and their bulk density diminishes. This finding is also consistent with theoretical predictions. Accounting for this correlation can reduce uncertainties in terminal velocities–size relations; however, it cannot be used for accurate predictions of such relations since changes in $\bar{A}$ for the same value of $\bar{D}_0$ can be more than a factor of 2 or 3. This variability indicates a spatial and temporal diversity of particle habits in natural ice clouds.

The radar estimates of V_Z and retrievals of cloud ice water content made with the radar-radiometer method can be used to derive empirical regressions between IWC and mass-weighted vertical velocities V_m. These relations are useful for climate models since IWC is a prognostic variable and realistic expressions for deriving sedimentation rate are largely unavailable. Depending on the cloud particle characteristic size and details of the particle size distribution, the ratio V_Z/V_m varies from about 1.3 to almost 2. The derived V_m-IWC regressions exhibit significant data scatter, but the scatter decreases with increasing cloud ice content. For a typical high-altitude ice cloud case from ASTEX we obtained the coefficient and the exponent in the V_m-IWC regressions 0.63 and 0.27, respectively, where IWC is in g m^{-3} and V_m is in m s^{-1}. The values of the coefficient and the exponent, however, vary from case to case quite significantly.

Acknowledgments. This research was funded in part through the NASA EOS Project Science Office and by the Environmental Science Division of the U.S. Department of Energy as part of the Atmospheric Radiation Measurements Program.

References

Atlas, D., M. Kerker, and W. Hitschfeld, Scattering and attenuation by non-spherical particles, *J. Atmos. Sol. Terr. Phys*., *3*, 108–119, 1953.

Atlas, D., S. Y. Matrosov, A. J. Heymsfield, M. D. Chou, and D. B. Wolff, Radar and radiation properties of ice clouds, *J. Appl. Meteorol*., *34*, 2329–2345, 1995.

Bohren, C. F., and D. R. Huffman, *Absorption and Scattering of Light by Small Particles*, 530 pp., John Wiley, New York, 1983.

Brown, P. R. A., and P. N. Francis, Improved measurements of the ice water content in cirrus using a total-water probe, *J. Atmos. Oceanic Technol*., *12*, 410–414, 1995.

Dowling, D. R., and L. F. Radke, A summary of the physical properties of cirrus clouds, *J. Appl. Meteorol*., *29*, 970–978, 1990.

Heymsfield, A. J., Ice crystal terminal velocities, *J. Atmos. Sci*., *29*, 1348–1357, 1972.

Heymsfield, A. J., and J. Iaquinta, Cirrus crystals terminal velocities, *J. Atmos. Sci*., *57*, 916–938, 2000.

Klimowski, B. A., et al., The 1995 Arizona Program: Toward a better understanding of winter storm precipitation development in mountainous terrain, *Bull. Am. Meteorol. Soc*., *79*, 799–813, 1998.

Kosarev, A. L., and I. P. Mazin, An empirical model of the physical structure of upper layer clouds, *Atmos. Res*., *26*, 213–228, 1991.

Kropfli, R. A., S. Y. Matrosov, T. Uttal, B. W. Orr, A. S. Frisch, K. A. Clark, B. W. Bartram, R. F. Reinking, J. B. Snider, B. E. Martner, Cloud physics studies with 8 mm wavelength radar, *Atmos. Res*., *35*, 299–313, 1995.

Matrosov, S. Y., Variability of microphysical parameters in high-altitude ice clouds: Results of the remote sensing method, *J. Appl. Meteorol*., *36*, 633–648, 1997.

Matrosov, S. Y., Retrievals of vertical profiles of ice cloud microphysics from radar and IR measurements using tuned regressions between reflectivity and cloud parameters, *J. Geophys. Res*., *104*, 16,741–16,753, 1999.

Matrosov, S. Y., A. J. Heymsfield, J. M. Intrieri, B. W. Orr, and J. B. Snider, Ground-based remote sensing of cloud particle sizes during the 26 November 1991 FIRE II cirrus case: Comparisons with in situ data, *J. Atmos. Sci*., *52*, 4128–4142, 1995.

Matrosov, S. Y., A. J. Heymsfield, R. A. Kropfli, B. E. Martner, R. F. Reinking, J. B. Snider, P. Piironen, and E. W. Eloranta, Comparisons of ice cloud parameters obtained by combined remote sensor retrievals and direct methods, *J. Atmos. Oceanic Technol*., *15*, 184–196, 1998.

Mitchell, D. L., Use of mass- and area-dimensional power laws for determining precipitation particle terminal velocities, *J. Atmos. Sci*., *53*, 1710–1723, 1996.

Orr, B. W., and R. A. Kropfli, A method for estimating particle fall velocities from vertically pointing Doppler radar, *J. Atmos. Oceanic Technol*., *16*, 29–37, 1999.

Petch, J. C., G. C. Craig, and K. P. Shine, A comparison of two bulk microphysical schemes and their effects on radiative transfer using a single column model, *Q. J. R. Meteorol. Soc*., *123*, 1561–1580, 1997.

Pruppacher, H. R., and J. D. Klett, *Microphysics of Clouds and Precipitation*, 714 pp., D. Reidel, Norwell, Mass., 1978.

Randall, D. A., Atlantic Stratocumulus Transition Experiment, *J. Atmos. Sci*., *52*, 2705–2706, 1995.

Stephens, G. L., First ISCCP regional experiment: Intensive field operations, II, *J. Atmos. Sci*., *52*, 4041–4042, 1995.

Starr, D. O'C., and S. K. Cox, Cirrus clouds, part II, Numerical experiments on the formation and maintenance of cirrus, *J. Atmos. Sci*., *42*, 2682–2694, 1985.

Stokes, G. M., and S. E. Schwartz, The Atmospheric Radiation Measurement (ARM) Program: Programmatic background and design of the cloud and radiation test bed, *Bull. Am. Meteorol. Soc*., *75*, 1201–1221, 1994.

A. J. Heymsfield, National Center for Atmospheric Research, Boulder, CO 80303.

S. Y. Matrosov, R/E/ET6, 325 Broadway, Boulder, CO 80303. (smatrosov@etl.noaa.gov)

(Received October 20, 1999; revised May 23, 2000; accepted May 28, 2000.)